Astronomical Capabilities of the Faint Object Spectrograph on Space Telescope

R. J. Harms and the FOS Science and Engineering Team

Center for Astrophysics and Space Sciences
University of California, San Diego
La Jolla, California 92093

Abstract

Examples of scientific observing programs planned with the Faint Object Spectrograph on Space Telescope are presented. An overview of the spectrograph design and operation is presented. The expected astronomical performance of the instrument is described in some detail. References for further information are given.

1.0 Introduction

The Faint Object Spectrograph (FOS) is designed to allow spectroscopic analysis of physical conditions in faint and often extremely distant astronomical objects. The Space Telescope (ST) itself provides unprecedented spatial resolution throughout the ultraviolet to near-infrared portion of the spectrum. The excellent image quality is used by the FOS not only to make possible study of fine structures but also to achieve major improvement in limiting magnitudes by suppressing sky background. As described below, the FOS design is matched to the ST-unique capabilities to provide astronomers a flexible instrument with broad spectral coverage, moderate spectral resolution, ultraviolet spectropolarimetry capability, stable and nearly linear photometric response over a large dynamic range, fine temporal resolution, and extremely low background.

Several examples of scientific studies planned by the FOS Investigation Definition Team (IDT) are mentioned in Section 2.0. These programs illustrate the intended applications of the FOS, but form a biased sample emphasizing the predominantly extragalactic interests of the FOS IDT. Section 3.0 describes the FOS design features, modes of operation, and its status as of June 1982. Of greatest interest to potential users, Section 4.0 discusses the anticipated performance of the FOS based on measurements of the flight hardware components. Finally, Section 5.0 lists references where the reader can obtain further information about the FOS.

The FOS is being built by the University of California, San Diego (UCSD) and prime subcontractor Martin Marietta Corporation (MMC) Aerospace Division in Denver, Colorado. Key personnel involved in the FOS program are introduced in Table 1.0-1.

TABLE 1.0-1
Principal FOS Scientists and Engineers

NAME	POSITION	INSTITUTION
Roger Angel	Co-Investigator	University of Arizona
Frank Bartko	Co-Investigator	Martin Marietta Corporation
Edward Beaver	Co-Investigator	Science Applications Inc., University of California, San Diego
Ralph Bohlin	Co-Investigator	Goddard Space Flight Center, Space Telescope Science Institute
Margaret Burbidge	Co-Investigator	University of California, San Diego
Arthur Davidsen	Co-Investigator	Johns Hopkins University
Holland Ford	Co-Investigator	Space Telescope Science Institute
Richard Harms	Principal Investigator	University of California, San Diego
Bruce Margon	Co-Investigator	University of Washington
Louis Ripp	Project Manager	Martin Marietta Corporation
Charles Ross	Project Manager	University of California, San Diego
Eugene Strein	Project Engineer	University of California, San Diego
Joseph Vellinga	Systems Engineer	Martin Marietta Corporation

2.0 Science programs

The light-collecting power of the ST in the ultraviolet spectral region, the sharp imaging capability, and the reduced sky background offer the potential for many exciting observations. In this section, we describe some of the programs planned by the FOS IDT.

Because this paper is primarily an instrumental description, the planned scientific investigations are presented only cursorily. Still, we hope some of the excitement is evident, while the examples illustrate uses of the FOS capabilities.

2.1 Active galaxies. High spatial resolution spectra of Seyfert and active galaxy nuclei are planned to obtain information concerning physical properties (temperatures, densities, and velocities) of the H II regions, dust content, and the nature of the ionization mechanism. Line strengths and profiles of the features listed in Table 2.1-1 will provide information to determine the physical parameters of individual ionized structures. Observations of intensity ratios of the auroral to transauroral line strength ratios listed in Table 2.1-2 will indicate dust content. Finally, measurements of the ultraviolet continuum and line intensities of differently ionized elements will indicate the extent of ionization due to thermal or nonthermal photoionization or due to shocks. All the lines in both tables lie within the spectral range accessible with the FOS.

TABLE 2.1-1
Density Sensitive Features

ION	WAVELENGTH (Å)	CRITICAL DENSITY*
[Ne V]	1575	2.0×10^8
[A V]	2691	1.1×10^8
[A III]	3109	5.8×10^7
[O III]	4363	2.4×10^7
[O III]	5007	6.5×10^5

* At $T = 10^4 K$

TABLE 2.1-2
Extinction Sensitive Transitions

ION	AURORAL/TRANSAURORAL WAVELENGTHS (Å)
[A III]	5192/3109
[A IV]	7300/2854
[A V]	4625/2691
[O II]	7320 - 7330/2470
[Ne III]	3342/1815
[Ne V]	2974/1575

2.2 Quasars. The studies of quasars are grouped in three categories below. The goals of these three broad programs can be summarized as: 1) determine the nature of underlying nebulosity associated with some quasars, 2) determine the physical conditions within quasars, and 3) seek the relationship of quasars with other astrophysical objects.

The spatial resolution of the ST will be exploited in order to analyze the nature of the underlying nebulosity seen around some quasars, and presumably to be seen around more quasars by the ST cameras. Spectra of this nebulosity will test the hypothesis that quasars are embedded in galaxies. The FOS design incorporates special occulting apertures matched to the ST optics to maximize the nebulosity signal to quasar plus sky background noise ratio for these observations. The FOS team also intends to observe asymmetrical wisps and jets associated with some quasars and to compare these data to observations of the optical synchrotron knots in the M87 jet. The ultraviolet continuum emission from the jets will test models which generate relativistic electrons by collision between relativistic protons and cooler denser gas. The data will also provide information about the synchrotron cutoff frequencies of the various knots.

The proposed investigation of physical conditions within quasars uses essentially the same methods as described in Section 2.1 to study Seyfert nuclei. In particular, we will obtain information concerning temperatures and densities from auroral and nebular line strengths, about dust content from auroral to transauroral line intensity observed ratios, and about the high density regions from density-sensitive transauroral line intensities. For highly redshifted quasars, the highly interesting helium abundances from measurements of He I and He II lines will be possible. Indeed, many extreme-ultraviolet lines of astrophysical significance will become observable in highly redshifted quasars. Table 2.2-1 lists some of these features along with the minimum redshift which will bring them into the observing range of the FOS on ST.

TABLE 2.2-1

Significant Quasar Features Observable with FOS for Restricted Redshifts

ION	REST WAVELENGTHS*(Å)	MINIMUM REDSHIFTS OBSERVABLE**
H I	1025.7, 972.5, ..., lim 911.8	0.12, 0.18, ..., 0.26
He I	584.3, 537.0, 522.2, lim 504.4	0.97, 1.14, 1.20, 1.28
He II	303.2, 256.3, 243.0	2.79, 3.49, 3.73
C II	1036.3+, 903.6++, ...lim 508.6	0.11, 0.27, ..., 1.26
C III	977.0, 386.2, 310.2, lim 259.0	0.18, 1.98, 2.71, 3.44
C IV	312.4, 244.9	2.68, 3.70
N I	1134.2++, 963.9++, lim 853	0.01, 0.19, 0.35
N II	1084.0++, 915.6++, 671.0++, 644.6++, ..., lim 418.9	0.06, 0.26, 0.71, 0.78, ... , 1.75
N III	989.8++, 763.3+, 685.0++, 451.9++, ..., lim 261.4	0.16, 0.51, 0.68, 1.54, ..., 3.40
N IV	765.1, 247.2	0.50, 3.65
O I	1039.2+, 1025.8+, 988.8+, lim 910.5	0.11, 0.12, 0.16, 0.26
O II	832.8++, 539.4++, 430.0++, lim 353.1	0.38, 1.13, 1.67, 2.26
O III	832.9++, 702.3++, 507.4++, 373.8++, 305.7, 303.6 2.76, 2.79	0.38, 0.64, 1.27, 2.08,
O IV	787.7++, 608.4+, 553.3+, 279.6+	0.46, 0.89, 1.08, 3.11
O V	629.7	0.83
O VI	1031.9, 1037.6	0.11, 0.11
Ne I	743.7, 735.9, lim 575.0	0.55, 0.56, 1.00
Ne II	462.4, 460.7, 454.6+, 445.0++, ..., lim 302	1.49, 1.50, 1.53, 1.58, ..., 2.81
Ne III	488.1++, 313.0+, 283.2++	1.36, 2.67, 3.06
Ne IV	543.9++, 542.1++, 541.1	1.11, 1.12, 1.13
Ne V	568.4++, 480.4++, 358.0++	1.02, 1.39, 2.21
Ne VI	558.6++, 433.2++, 401.1++, 399.8++	1.06, 1.65, 1.87, 1.88
Ne VII	465.2	1.47
Ne VIII	780.3, 770.4	0.47, 0.49
Na II	376.4, 372.1, 301.4, 300.2, lim 262	2.06, 2.09, 2.82, 2.83, 3.39
Na III	378.1	2.04
Na IV	410.4, 408.7	1.80, 1.81
Na V	463.3, 461.0, 451.9	1.48, 1.49, 1.54
Na VI	489.6, 414.3, 311.9	1.35, 1.78, 2.69
Mg II	lim 824.7	0.39
Mg IV	321++	2.58
Mg V	353.1, 351.1	2.26, 2.28
Mg VI	403.3, 400.7, 399.3	1.85, 1.87, 1.88
Si II	lim 759	1.52
Si III	566.5, lim 370	1.03, 2.11
Si IV	457.7, lim 275	1.51, 3.18
S II	912.7, 910.5, 906.9, lim 530	0.26, 0.26, 0.27, 1.17
S III	1021.2, 1015.5++, 1012.5, 735.3, 732.4, lim 354	0.13, 0.13, 0.14, 0.56, 0.57, 2.25
S IV	1073.2, 1062.7, 816.0, 809.7, 753.8, 750.2, 748.4, 744.9, 661.4, 657.3, lim 262	0.07, 0.08, 0.41, 0.42, 0.53, 0.53, 0.54, 0.54, 0.74, 0.75, 3.39
S V	786.5	0.46
S VI	944.5, 933.4, 249.3, 249.0	0.22, 0.23, 3.61, 3.62
A I	1066.7, 1048.2, 894.3, 876.1, lim 786.8	0.08, 0.10, 0.29, 0.31, 0.46
A II	932.0, 919.8, 740.3, 723.4, 671.9, 670.9, 666.0, 661.9, lim 449	0.23, 0.25, 0.55, 0.59, 0.71, 0.71, 0.73, 0.74, 1.56
A III	887.4, 878.7++, 871.1, 637.3, lim 303	0.30, 0.31, 0.32, 0.80, 2.80
A IV	850.6, 843.8, 840.0	0.35, 0.36, 0.37
A V	449.1	1.56

* Blends unresolved by FOS listed at weighted line center

** FOS minimum observable wavelength = 1150Å due to magnesium fluoride cutoff

\+ Lowest wavelength of marginally resolvable blend with FOS

++ Lowest wavelength of a blend only partially resolvable by FOS

NOTE: References for the wavelengths are from National Bureau of Standards (1950), Chemical Rubber Company (1968), Osterbrock (1974), and Bahcall (1979). The data given are sometimes inconsistent but never to a degree which significantly undermines the intent of the table to specify redshift limits for FOS observations.

A specific program to test the hypothesis of cosmological redshifts for quasars involves correlating equivalent widths of the Lα and C IV lines with the far-ultraviolet continuum luminosities of quasars. Presently only high redshift quasars can be observed;

the ST allows low redshift observations in the ultraviolet which should decide the nature of the correlation. We also plan to test for the same correlation in Seyfert galaxies, which if found, would establish both a relationship between quasars and Seyferts as well as the cosmological redshift hypothesis for quasars.

2.3 Galaxy chemical abundances. The FOS IDT has proposed observations of H II regions and planetary nebulae in the Local Group Galaxies in order to determine young and old stellar population abundances respectively as a function of galaxy mass and location within a galaxy. The spatial resolution of the ST will allow extension of these abundance measurements well into the nuclei of these galaxies, while absence of Hg I λ4358 airglow will make possible the detection of far fainter O III λ4363 abundance sensitive (through electron temperature) line intensities than is possible from the ground. Also, observed line strengths of ultraviolet lines such as C IV λ1548 will permit abundance determinations of astrophysically important elements.

2.4 Planetary nebulae. We have proposed to obtain ultraviolet spectra of the central stars of planetary nebulae in the Magellenic Clouds. The well-determined distances will allow accurate luminosities to be derived. The long-baseline ultraviolet spectra should provide good data for fitting model stellar atmospheres from which accurate effective temperatures can be obtained. It will be possible to observe central stars of planetary nebulae ranging in brightness from V = 15.6 to V=22 which will define central star evolution over a period in excess of 30,000 years.

2.5 Time resolved spectrophotometry. Time resolved spectrophotometry of binary X-ray sources at ultraviolet and optical wavelengths can be expected to detect pulsations which will reveal the physical processes occurring when a relatively cool stellar atmosphere is intensely irradiated with X-rays. A series of spectrophotometric data from an X-ray binary serves both to elucidate the physics of the X-ray to optical pulse processing mechanism and to provide a velocity curve for the cool stellar companion from which (with the X-ray source velocity profile) the masses of the cool and X-ray emitting objects can be calculated. This program takes advantage of the FOS capability to obtain spectra at intervals as short as every 30 milliseconds.

Two additional results will be obtained from the data gathered for the program above. Time-integrated spectral profiles at moderate dispersion will discriminate between Roche lobe overflow and stellar wind driven mass transfer processes. Significant lines for this work are C IV λ1548, N V λ1240, and O VI λ1032 (the last not obtainable with the FOS). The second result to be expected from these data is the detection of absorption lines of the X-ray ionized surrounding matter providing information about the X-ray luminosity, circum-source matter density, and the flux variability of galactic X-ray sources on time scales comparable to the recombination times of the nearby interstellar gas -- about 100 years.

A similar study of recently discovered extreme ultraviolet sources such as HZ 43 and Feige 24 should help determine the high temperature end of the degenerate star luminosity distribution. The important inferences on stellar evolution provided by such data will comprise an interesting new test of the weak interaction theory.

2.6 FOS spectropolarimetry. Interstellar polarization was discovered in visible light 30 years ago and within a few years the basic explanation used today had been developed. The angular momentum vectors of spinning elongated or flattened dust particles are aligned in a perpendicular direction by an interstellar magnetic field. Thus the mean grain profile is elongated and the interstellar medium containing thin grains is linearly dichroic. In the 1960's it was found that the wavelength dependence of the linear polarization could be explained by grains of about the same size as those responsible for optical interstellar extinction and so a unified picture emerged. The subsequent discovery of circular polarization tended to confirm this picture.

However, satellite measurements of interstellar extinction in the ultraviolet have revealed added complexity (e.g., Aannestad and Percell, 1973). Two additional grain components seemed to be required -- one to explain the 2200Å extinction peak and another - very small particles - to account for the continued rise in extinction in the far ultraviolet. There are regional variations in the amount of ultraviolet relative to optical extinction. An understanding of the nature of these grain components is an essential prerequisite to elucidating the origin of interstellar dust.

Ultraviolet spectropolarimetry of reddened early type stars will be important in unraveling various aspects of these mysteries. First, the graphite explanation of the 2200Å feature is problematical and will suffice only if the particles are small and virtually spherical (Gilra, 1972). Since spherical particles produce no interstellar polarization, a clear test of this hypothesis is presented. Second, the composition of the very small particles is unknown though it has been suggested that they are the

refractory cores around which the classical dielectric particles accrete. Are these grains elongated and aligned? Only ultraviolet polarization measurements can answer this since small particles produce negligible affects at optical wavelengths. The details of grain alignment mechanisms are still controversial and here we have an unparalleled opportunity to discover many size and composition dependent effects.

Stars other than those exhibiting optical interstellar polarization will also be polarized in the ultraviolet. Electron scattering is important in Be and Of stars. Late type supergiants are also bright enough to be detected. The origin of polarization is a matter of debate; although circumstellar dust seems to play an important role, photospheric effects are also in evidence. Ultraviolet polarimetry will help determine the relative importance of these mechanisms. Compact reflection nebulae can also be examined to find the size and composition of dust.

A completely different mechanism giving rise to linear polarization is the influence of very strong magnetic fields on radiative transfer through the atmosphere of a white dwarf. It is expected that for light frequencies higher than the cyclotron frequency, the linear polarization will not propogate through the atmosphere (Angel, 1978). A cutoff in polarization at short wavelengths thus would give a fairly direct measure of field strength. The strong surface field measurement (by the Zeeman effect) of 2.5×10^8 G in Grw + 70° 8247 implies a cyclotron frequency corresponding to a wavelength of 4000Å. A drop in linear polarization is seen below this wavelength and measurements below 3000Å should show no recovery. If the effect can be calibrated and checked in well understood objects, determination of polarization cutoff can be used to give a unique measure of field strength in other strongly magnetic white dwarfs.

Another important area of exploration with the FOS polarimeter will be the polarimetric properties of quasars and Seyfert galaxy nuclei using both the ultraviolet response and good spatial resolution of ST. In nearby Seyfert nuclei the forbidden line emission regions just revolved spatially from the ground will be easily resolved the the ST. In NGC 1068, for example, asymmetric dust clouds exterior to the permitted line emission region give rise to strong (10%) net polarization at 3000Å. The wavelength dependence further into the UV will give information on the dust composition, and its spatial and spectral distribution will help show the geometry and dynamics of the galactic nucleus. For the majority of quasars whose polarization is detected, but quite small (about 1%), it is not even known whether scattering processes or synchrotron radiation is responsible. The fact that in radio quasars with double lobes, the polarization and lobe axis are aligned, suggests that the origin is related fairly directly to the quasar geometry. We can expect that studies with the FOS polarimeter and from the ground covering the range 1200Å through the near infrared may lead to an understanding of the origin of polarization and perhaps of the continuum emission itself.

2.7 Cosmology with supernovae. One of the most exciting and difficult observations planned with the FOS will be to obtain spectrophotometric measurements of distant (redshift $\simeq 0.3$) supernovae in an attempt to determine the cosmological parameter q_o. (This presumes use of similar observations for lower-redshift supernovae to measure H_o.) The concept has been thoroughly discussed in the literature (Wagoner, 1980 and references therein).

The basic idea is simple. If it is possible to measure the cosmological redshift (from that of the containing galaxy), the initial time of explosion (early detection), and the expansion velocity of the supernova photosphere, then the physical size of the emission region can be known as a function of time (practically, limited to an interval about one month). Spectrophotometry combined with sufficient supernova models can fix the observed luminosity. (If the supernova were simply a blackbody, the derivation would be trivial; one obtains apparent luminosity directly, while the spectrally measured temperature and known physical dimensions determine absolute emitted luminosity. The true situation is, of course, more complex.)

Severe theoretical difficulties arise from the uncertainties introduced by intervening interstellar extinction and a complex photosphere (whose effective radius may vary with wavelength). However, the large sampling of information obtained from a given observation (hundreds to thousands of sampled wavelengths) probably can overcome these difficulties. The procedure is especially attractive, however, because cross-checking is available; successive measurements in time sample the supernova at different sizes and temperatures. Of course, observations of several supernovae will be necessary also.

The practical difficulties are also major. At a redshift of 0.3, the blue magnitude of a supernova will be about B = 22 to 23, and its temperature around 15,000K shortly after formation. In one month, it will cool to about 6000K and fade a magnitude. As described in Section 4.0, such an object will be possible but difficult to observe at moderate resolution with the FOS; especially as the supernova fades, it may be necessary to switch

to a low dispersion. In order to reduce the background from the parent galaxy, the ST spatial resolution is clearly essential. (However, we expect detection of the supernovae to arise from ground-based automated monitor surveys.)

It is fair to say that these measurements of redshift 0.3 supernovae lie at the extreme limits of ST + FOS performance. However, success appears possible, and the scientific reward will be large. Astronomers being ever willing to push instrumentation to its limits, we have no doubt others will conduct even more challenging observations on ST.

3.0 Instrument description

The Faint Object Spectrograph is one of four axial scientific instruments on the Space Telescope. Figure 3.0-1 depicts the main features of the FOS. The instrument is divided into two major compartments: an electronics shelf area above and an optics-plus-detector region below. The entire structure is about 1 x 1 x 2 meters.

Light enters the FOS through a pair of entrance ports (shown at lower left of Figure 3.0-1) located about 60mm = 215 arcseconds off the optical axis of the ST. The light from the object of interest then passes through one of two independent optical channels, each of which focuses nearly stigmatic spectral images on the photocathodes of photon-counting Digicon detectors. These channels differ only in the wavelength sensitivity of their respective detectors. At the ST focal surface is placed the FOS aperture wheel, containing eleven sets of single or paired apertures which range in size from 0.1 to 4.3 arcsec projected onto the sky. The optical beam then passes through the polarization analyzer (which includes a clear aperture position). The grazing incidence mirror, a "roof" prism, deflects the beam 22° upward. The reflection is required in order to allow the apertures to be placed near ST optical axis to minimize astigmatism, while meeting packaging constraints within the FOS. The deflected beam passes through an order-sorting filter, when required, in the filter/grating wheel. It is collimated by an off-axis paraboloidal mirror and then both dispersed (except for one imaging position) and focused by the selected element on the filter/grating wheel.

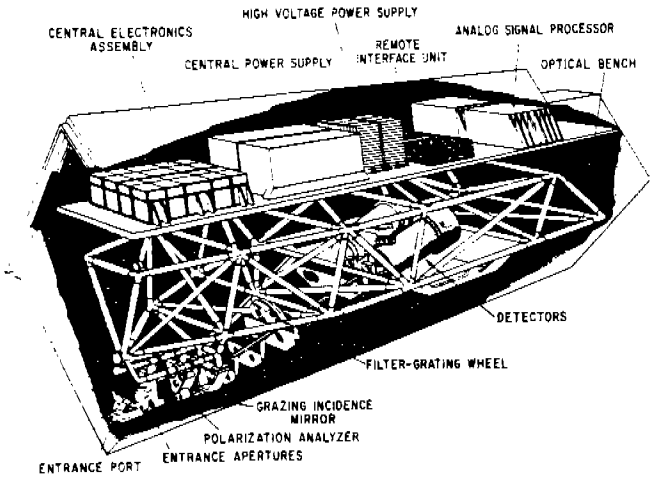

FIGURE 3.0-1. Faint Object Spectrograph: dimensions of the axial ST instrument are about 1 x 1 x 2 meters.

3.1 Optics. The design of the FOS optics is dominated by the desire to maximize throughput efficiency while utilizing the part of the ST focal plane as nearly on-axis as possible. The FOS design has eliminated any need to compensate for ST optical distortions, and has reduced to a minimum the number of optical surfaces. For example, a far-ultraviolet photon suffers only 3 reflections in the FOS before reaching a detector (grazing-incidence mirror, collimator, and focusing grating).

The entrance port has simply two positions to close or open the FOS to external light. The port mechanism also contains mirrors so that, in its closed position, light from the internal spectral calibration lamps can be shone through the optical path for wavelength calibrations.

The entrance aperture mechanism selects one of the twelve aperture sets (in either optical path). Table 3.1-1 lists the various aperture choices provided. The largest aperture, 4.3 arcseconds square, will be used for target acquisition. A variety of apertures from 0.1 arcseconds diameter for spectroscopy of fine spatial structure (e.g. knots in jets such as in M87) to 1.0 arcseconds for spectrophotometry or faint-nebula spectroscopy will enable astronomers to conduct diverse observations with high scientific efficiency. Specialized occulting apertures are intended for the study of faint sources

surrounding bright objects, particularly nebulosity surrounding quasars.

Table 3.1-1 Primary Entrance Apertures

Number	Shape	Size* (arcsec)	Center-to Center Separation(arcsec)	Special Purpose
Single	Round	0.5 dia	N/A	Polarimetry
Single	Round	0.3 dia	N/A	Polarimetry
Single	Round	1.0 dia	N/A	Polarimetry
Blank	N/A	N/A	N/A	Light Shield
Single	Square	4.3	N/A	Target Acquisition
Pair	Square	0.5	3.0	Object & Sky
Pair	Square	0.25	3.0	Object & Sky
Pair	Square	0.1	3.0	Object & Sky
Pair	Square	1.0	3.0	Object & Sky
Single	Rectangular**	0.25 x 2.0	N/A	Extended Objects
Single	Square	2.0	N/A	Surrounding Nebulosity
Single	Rectangular**	0.7 x 2.0	N/A	Surrounding Nebulosity
		Failsafe Entrance Aperture		
Pair	Square	0.5 and 4.3	4.4	Target Acquisition & Spectroscopy

* For rectangular apertures, first dimension is along dispersion, second perpendicular to dispersion.

** With occulter bar which is 0.3 arcsec wide in cross-dispersion direction.

The FOS polarization analyzer allows positioning of any of three elements into either optical path: a clear aperture, a thin-waveplate plus Wollaston prism assembly, or a thick-waveplate plus Wollaston prism assembly. One waveplate is permanently located in front of each Wollaston. The polarimeter is designed so that only a single motor is required to rotate the waveplates and to move either of the Wollaston/waveplate pairs from one entrance port to the other or out of the way. A drum, which is only 1.9 inches in diameter, contains the two Wollaston/waveplate pairs. The Wollastons are permanently fixed to the drum, but the waveplates are mounted in rotatable cylinders inside the drum. The waveplate cylinders have a 16-tooth gear on the outside which meshes with a 17-tooth fixed center gear inside the drum. One revolution of the drum rotates the Wollastons by 360°. The waveplates, however, rotate 382.5°. Each rotation of the drum thus increments the position angle of the waveplate fast axis by a net 22.5°. Sixteen rotations of the drum bring the mechanism back to its original configuration. Figure 3.1-1 is a photograph of the flight polarizer mechanism.

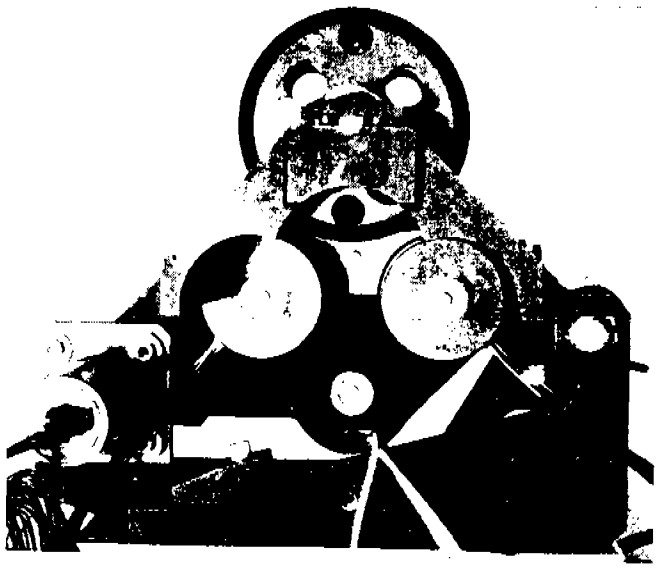

FIGURE 3.1-1. FOS Polarizer Analyzer: upper rotating barrel is about 5 cm diameter.

The filter/grating wheel photographed in Figure 3.1-2 (still with dummy optical elements), allows selection from ten positions in each optical path. Table 3.1-2 presents the dispersion selections available, and describes the filters used in five of the ten positions.

A considerable challenge in the FOS design was the requirement to maintain positional tolerances (initial alignment and stability) in the tens of micrometers for an optical structure over a meter long. Not surprisingly, the FOS optical bench is made of graphite-epoxy. However, as a photograph of the bench (Figure 3.1-3) and a photograph of its joints (Figure 3.1-4) make clear, the geometry is complex. The design selected uses pre-welded invar joints into which are inserted the graphite-epoxy tubes, all designed for near-zero thermal expansion coefficient at the optical compartment operating temperature of 20C.

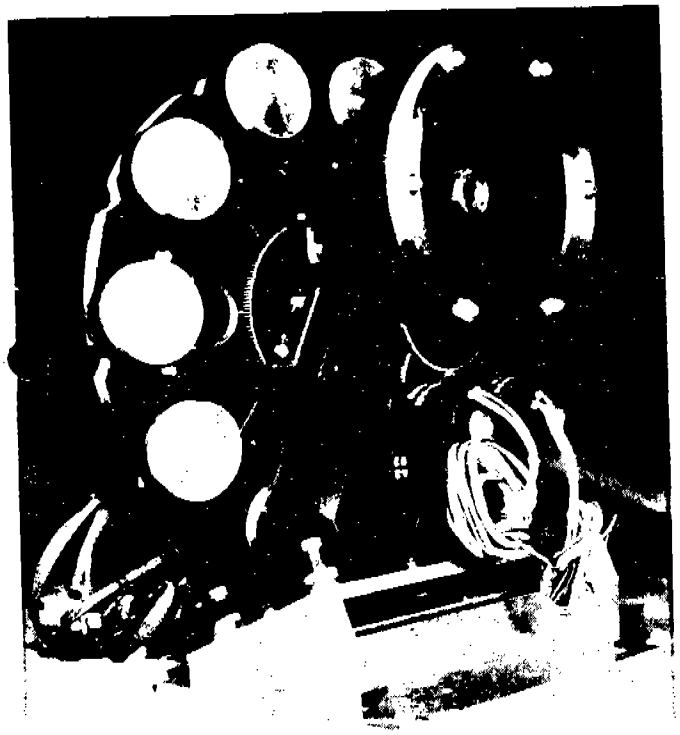

FIGURE 3.1-2 (upper left). FOS Filter/Grating Wheel: outer ring of aluminum caps are disperser locations; inner ring of holes are filter locations.

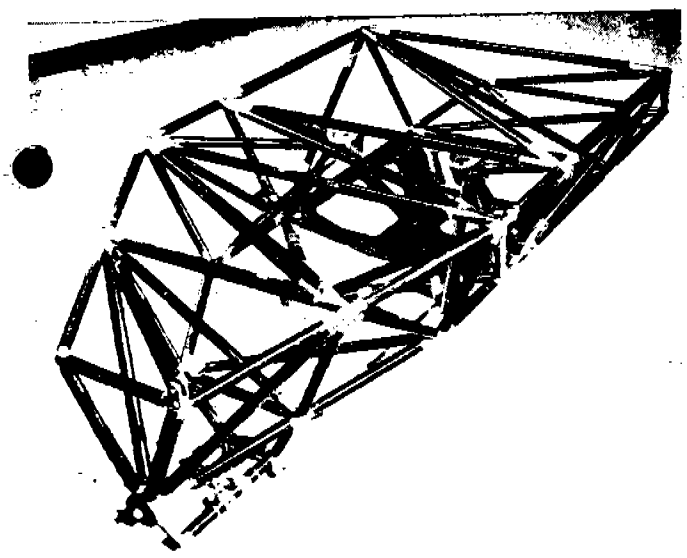

FIGURE 3.1-3. FOS Optical Bench: over one meter long, constructed of invar joints and graphite-epoxy tubes.

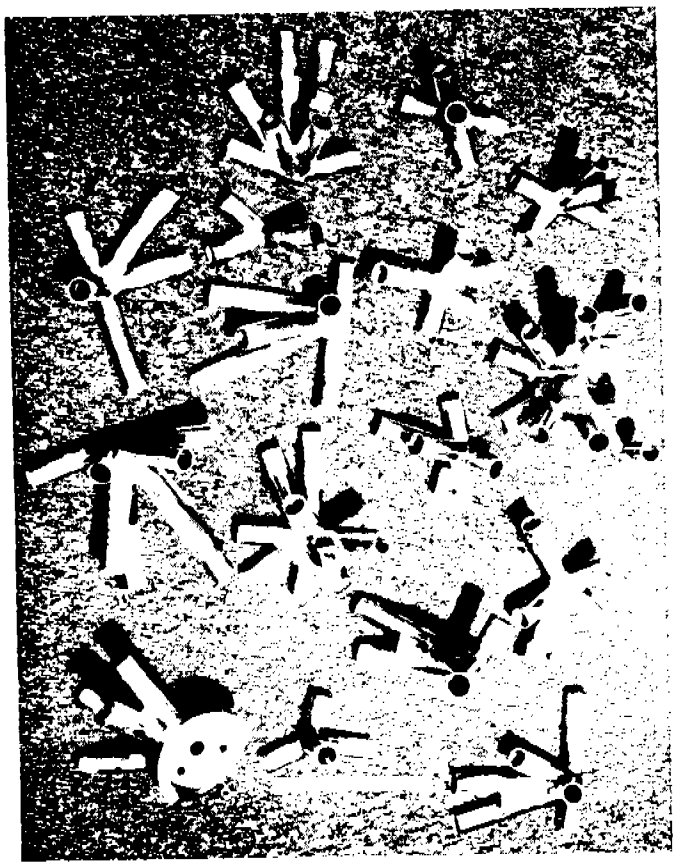

FIGURE 3.1-4. Optical Bench Invar Joints: note geometrical complexity leading to choice of welded joint structure.

Table 3.1-2 Wavelength Coverage of FOS Modes

Dispersers

Element	Resolution at Central Wavelength ($R = \lambda/\Delta\lambda$)	Wavelength (nm) Min	Max
Grating H13	1200	110	164
Grating H19	1200	153	228
Grating H27	1200	221	329
Grating H40	1200	319	474
Grating H57	1200	459	683
Grating H78	1200	626	931
Grating L16	200	110*	220**
Prism	100	250	700
Grating L60	200	400	800
Mirror	1	110	900

Blocking Filters

Element	Wavelengths (nm) T=1%	T=90%	Minimum Wavelength (nm) Mode	Transmission at Min. Wavelength
FH27 = fused silica	>165	<200	221	93%
FH40 = WG 305	290	340	319	87%
FH57 = GG375 G34	355	425	459	91%
FH78 = OG 530	510	550	626	91%
FL60 = CG375 G34	355	425	400	85%

* Resolution is about 400 at 250 nm.
** Resolution is about 25 at 700 nm.

3.2 Detectors. There are two independent assemblies, one for each optical channel. Each detector assembly consists of a Digicon tube (described in Harms et al., 1979 and references therein), deflection coils, a permanent magnet focus assembly, magnetic shielding, mounting and alignment structure, heat pipes, temperature sensors, hybrid preamplifiers, and connectors.

The two Digicon detector assemblies, designated "red" and "blue", differ only in their photocathode and faceplate materials. The blue detector has a bialkali photocathode (Na_2KSb) deposited on a magnesium fluoride window to cover the wavelength region 115 nm $< \lambda <$ 500 nm. The photocathode of the red detector, trialkali $Na_2KSb(Cs)$ deposited on fused silica, provides an extension of sensitivity to the red, covering the range 180 nm $< \lambda <$ 850 nm. To reduce dark background to the extremely low values required for FOS scientific programs (< .002 counts diode^{-1} sec^{-1}), the detectors are cooled to the temperature range -10C to -28C by means of attached heat pipes.

The Digicons operate by accelerating (to 20-25 KeV) photoelectrons emitted by the transmissive photocathode onto a linear array of 512 silicon diodes. Figure 3.2-1 shows a photograph of a (reject) diode array mounted onto its 5 cm diameter ceramic header containing 520 vacuum-tight electrical feedthroughs. The charge pulse generated in each diode is amplified and counted by one of 512 independent electronic channels, beginning with the hybrid preamplifiers physically colocated with each Digicon. Figures 3.2-2 and 3.2-3 are photographs of the red flight detector, showing the overall detector assembly and the preamplifiers at the aft end.

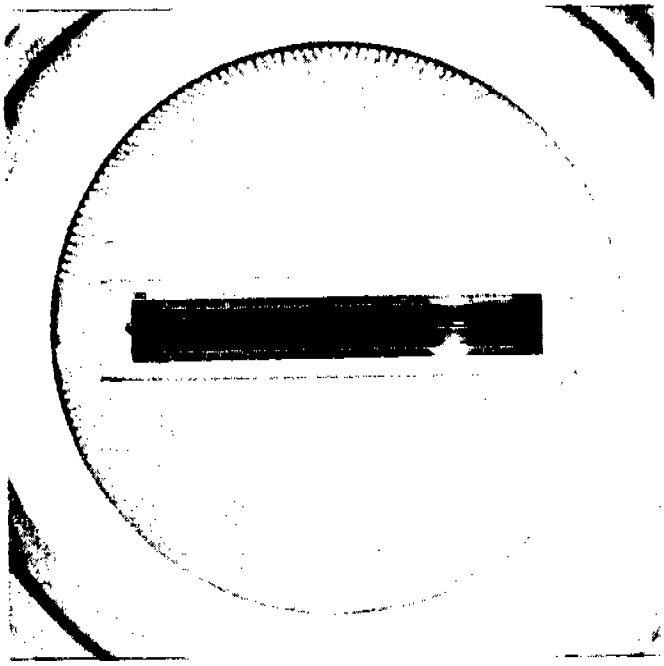

FIGURE 3.2-1. Digicon Array on Ceramic Header: 512-element array is about 2.5 cm long; 5 cm diameter header contains 520 vacuum feedthroughs.

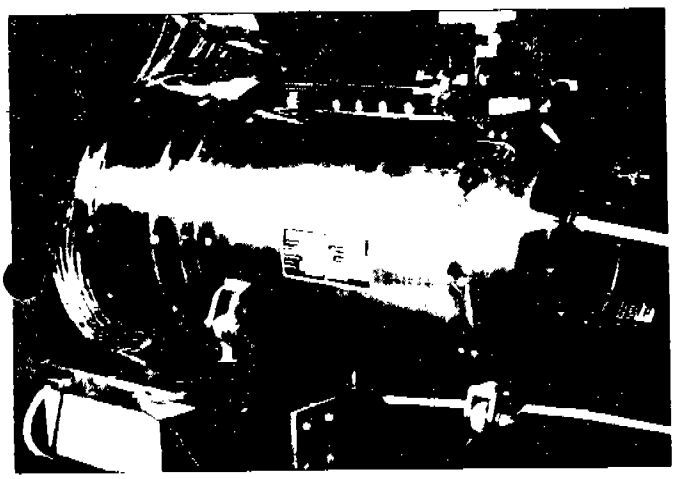

FIGURE 3.2-2. Red Flight Detector: during single-string integration tests at UCSD, 511 of 512 channels are operating.

FIGURE 3.2-3. Detector Hybrid Preamplifiers: the 512 preamps fit into back end of detector assembly; set consumes less than 10 watts.

3.3 Control. The FOS receives commands processed through the ST Command and Data Handling (C&DH) computer which controls all ST scientific instrument activity. Internal to the FOS itself are two microprocessor systems, one for each detector system. Each microprocessor (only one can be operating at a given time) controls all the functions needed to operate one side of the FOS such as moving mechanisms, controlling power supplies, scanning the photocathode with the diode array by use of the deflection coils, and accumulating science data. The memory for each microprocessor consists of 24K bytes of read-only memory and 32K bytes of random-access memory. Figure 3.3-1 details the memory usage early in 1982 (still subject to minor evolution). Storage available for science data integration during an observation is adequate for 12K 16-bit data elements, allowing considerable (but finite!) scanning flexibility with the 512-element diode arrays. (The firmware plot packages have been essential for the development and ground-based testing of the FOS.)

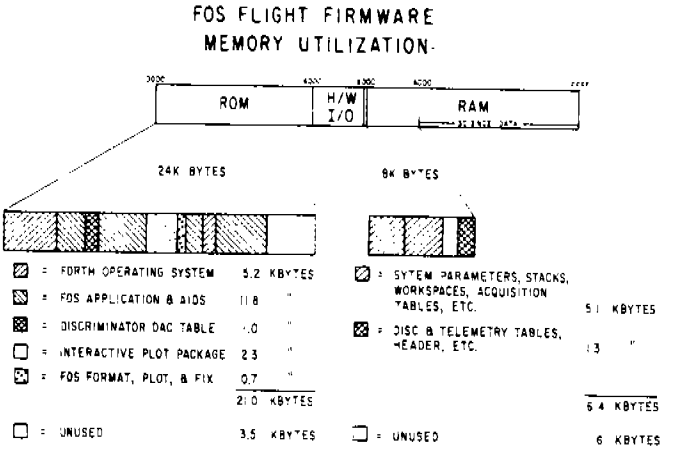

FIGURE 3.3-1. FOS Onboard Control Firmware.

3.4 Operating modes. Because so many FOS parameters are software-selectable under ground-system commands, the possible number of observing configurations truly is astronomical. However, in terms of intended use, the FOS operates in one of six basic modes: 1) target acquisition, 2) spectroscopy, 3) time-resolved, 4) sectropolarimetry, 5) rapid-readout, and 6) time-tagged. Each offers the observer unique advantages (and limitations) for specific purposes.

As might be suspected, acquiring an extremely faint astronomical target in a viewing field of maximum size 4.3 arcseconds square using a one-dimensional detector, can be a nontrivial task. The preferred solution, which should become the usual procedure with increasing ST experience in orbit, will be to know target coordinates and possess ST pointing of sufficient accuracy to allow simply commanding the telescope to the proper position to image the object into the desired FOS entrance aperture. For less benign circumstances, the FOS possesses one position on the filter/grating wheel with a mirror only to provide undispersed images on the detectors as well as onboard software and firmware able to determine small offsets necessary to center a target in a particular FOS aperture, provided that the field is extremely simple. If locating the target requires application of more than the most rudimentary intelligence, the onboard software simply maps the field and depends upon the astronomer (working with the ground data display system) to identify the desired target. The time to acquire a faint target in a complex field can easily be greater than the exposure time to obtain the spectrum; thus, blind offsetting techniques such as are used at ground-based telescopes will be desirable for increased observing efficiency. It is also possible, though not assured, that one of the two ST cameras can be used to assist in target acquisition for the FOS.

The most common use of the FOS will probably be in the spectroscopy mode. Any one of ten possible portions (Table 3.1-1) of the ST image can be usefully observed in any of nine spectral regions (Table 3.1-2). Observations may be virtually as brief as desired (shortest snapshot is less than 50 msec) or as long as the time-allocation committee will approve. For a typical observation, lasting from a few minutes to a few hours, the data is internally integrated in the FOS in software selectable intervals (now planned to be one minute) between each readout to the ground or ST tape recorders. The frequent readouts result in negligible loss of observing efficiency and protect against catastrophic losses of data.

The time-resolved mode will be used to study objects with known periodicity in about the 50 msec to 100 second range. In this mode, the data is stored in separate memory

locations (slices) corresponding to phase, with four to ten samples per full period being typical. Interruptions of data acquisition to read out each frame of data are set by commands to last an integral number of periods so that each frame of an observation has the same correspondence between phase and slice (so long as the period is correctly known!). Thus, all information should be contained in the last frame. Finally, there exist synchronous and asynchronous submodes; these differ only as to whether or not the initial phase angle is explicity locked to the source at the start of the observation (by commanding the start to occur at a specified Universal Time).

The technique used for spectropolarimetry in the FOS is very similar to that developed for ground-based instruments. A polarizing prism of doubly refractive material is introduced into the spectrophotometer, so as to form twin dispersed images of the slit in opposite senses of polarization at the detector. This analyzer is used at a fixed position, and a waveplate is introduced ahead of it which is turned in 22.5° intervals to analyze for linear and circular polarization. In this way the polarization effects in the dispersing optics following the analyzing prism are of no consequence, and have no effect on the accuracy of the measurement. Two separate waveplates of differing retardation are included in order to allow measurement of linear and circular polarization throughout the ultraviolet region. (It turns out that this allows visible-light operation also.) Any spectral mode may be used with either polarizer waveplate.

There are certain astronomical targets where rapid time variability is suspected, but the precise period of variability is unknown, or aperiodic rapid variabiity is expected. Time-resolved mode is unsuitable for these observations, as the bin folding period must be preset in that mode. Instead, normal FOS data taking is used, but the spectra are read out at very frequent intervals, rather than the approximately 60-sec integration times we anticipate for normal FOS data-taking. The frequency of readout is again set by the observer's requirements, but the shortest possible integration times are limited by various processor overheads. We expect 20 ms is a reasonable estimate of the shortest integrations (the exact minimum overheads are complex because the possibility exists to take "short spectra", ignoring some of the 512 diodes). This rapid-readout capability obviously requires the 1 MHz downlink from ST through TDRSS to the ground (or storage onto magnetic tape within ST).

The time-tagged mode, probably to be the least used FOS mode, will allow study of the most rapid variability possible using the FOS. Periodic or aperiodic variability on timescales in the range of about 10 microsec to 50 msec are well suited to time-tagged study. In time-tagged mode, each of the FOS accumulators counts the 1.024 MHz spacecraft clock rather than sensor counts. When the first photon arrives in a given channel, this counting freezes and further counts are inhibited in that channel. To be of value, time-tagged mode data must normally be read out at high rates, e.g., the 1 MHz telemetry rates, and will produce a very high data rate during its rare usages (estimated 2%-5% of FOS observing time). Note that this produces far more than 2%-5% of FOS data, however; it may (in competition with rapid-readout mode) produce a majority of FOS data to be reduced. The data outputs are each unsigned integers between 0 and 65,535. The selected accumulation time, for reasonable data, must be long enough to allow proper flight software operation, but be less than the clock overflow period, resulting in a range of allowed periods from about 10 msec to 64 msec. The data obtained in this mdoe will be similar in format to that obtained by many X-ray experiments.

3.5 Schedule. The FOS was selected to be a first-generation instrument aboard ST in November 1977, and will be delivered to NASA in April 1983 to support the planned early 1985 launch date for ST. At the time this paper is being written (June 1982), the design of the FOS and the fabrication of all flight hardware components has been completed. Assembly of the instrument is underway (Figures 3.5-1 to 3.5-7), with alignment and acceptance tests soon to follow. Measurements of the flight components have been completed, allowing realistic prediction of the performance to be expected of the FOS in the ST.

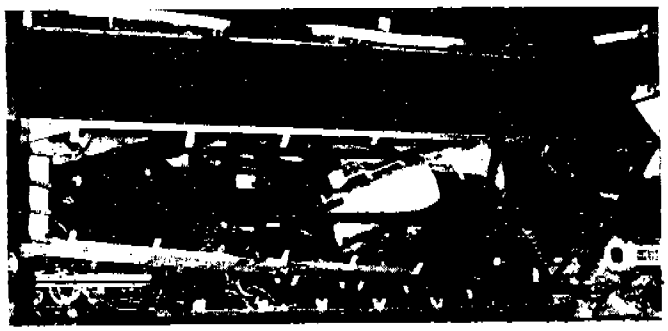

FIGURE 3.5-1. Optics/Detector Compartment during assembly.

FIGURE 3.5-2. FOS Structure being assembled in its transport frame.

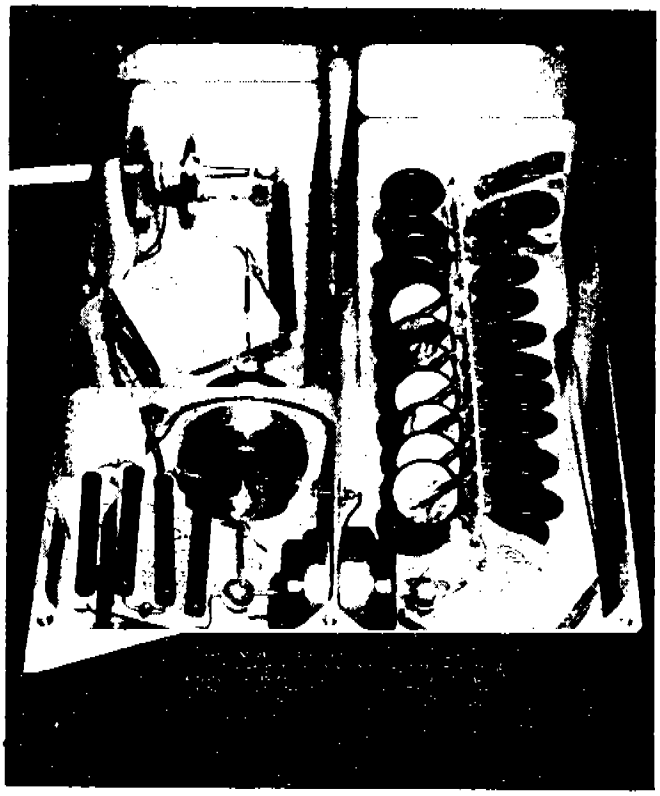

FIGURE 3.5-3. FOS High Voltage Power Supply partially assembled early 1982.

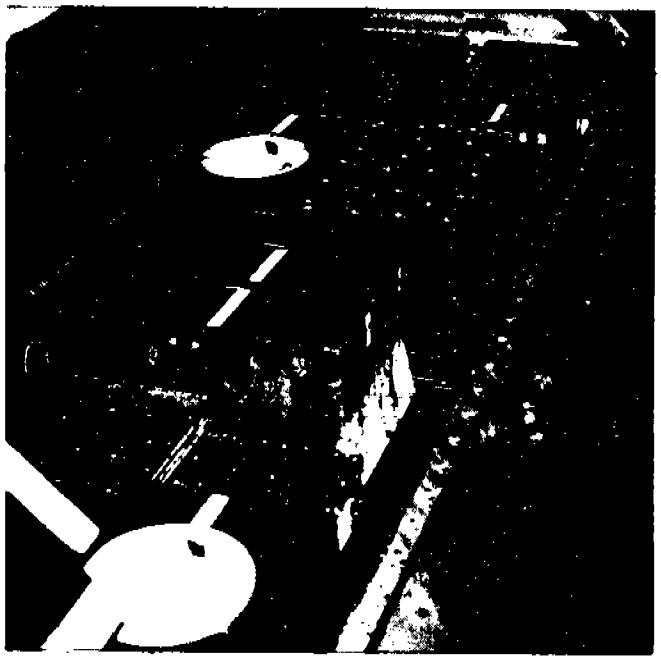

FIGURE 3.5-4. Electronics Bench during assembly.

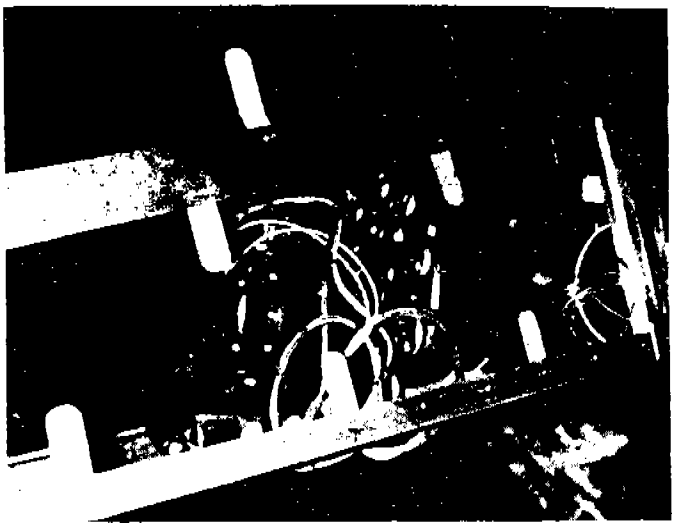

FIGURE 3.5-5. Filter/Grating Wheel being assembled onto optical bench.

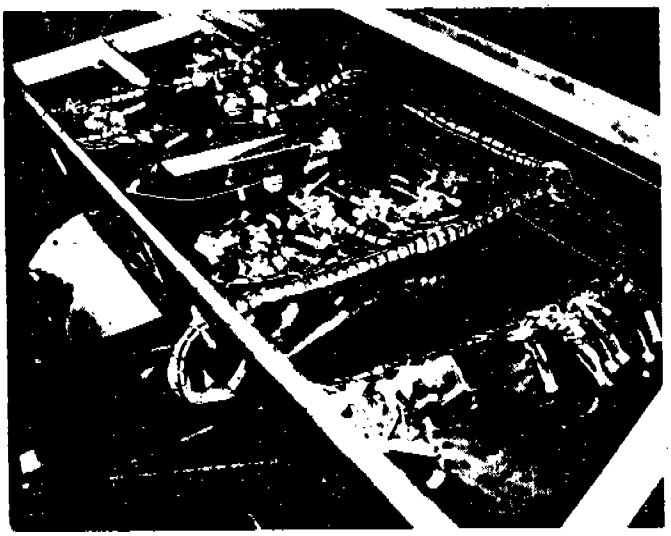

FIGURE 3.5-6. Flight Harness installation, optics bay below, electronics shelf foreground.

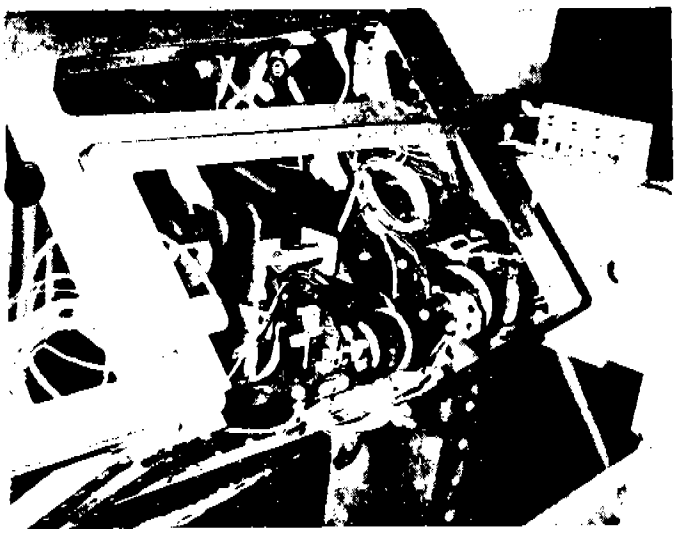

FIGURE 3.5-7. Polarizer and Entrance Port Mechanisms assembled into the FOS.

4.0 Performance

Knowledge of expected performance parameters for the FOS in ST which should prove valuable for planning observing programs are presented in this section. As will be evident, the FOS promises to be a flexible instrument applicable to observations over a wide range of luminosities, including especially faint objects as its name suggests.

4.1 Noise. In order to achieve faint limiting magnitudes, extreme reduction of instrumental background noise sources is essential. The favorable pulse-height-distribution of the Digicons makes false counts due to random analog signals exceeding the discriminator threshold very rare (approximately one such false count per Hubble time constant). The noise sources which can be significant to the FOS are: 1) straylight, 2) fluorescence and phosphorescence due to energetic particle bombardment, 3) thermionic emission, and 4) electromagnetic interference.

The ST itself includes many safeguards against straylight--sun shield, baffles, and high quality optics. The FOS apertures limit incoming light, filters block unwanted short-wavelength photons, while internal baffling must suffice to control other straylight. Unfortunately, no measurements of straylight performance are yet possible, and predictions of straylight performance are not to be trusted (in this author's opinion). Of course, we intend and expect that for most observations straylight will not be a limiting factor. One likely exception can already be identified. Because the FOS is a single-pass spectrometer with broad wavelength sensitivity, ultraviolet spectra of very red objects may suffer strong red straylight contamination. Fortunately, for such observations, the High Resolution Spectrograph can be used.

The sapphire prism and the windowed detectors each contribute unwanted counts due to fluorescence and phosphorescence under energetic-particle bombardment such as will be seen in orbit. Due to this concern, we have measured the light-producing properties of the materials used to manufacture the FOS. Major lot-to-lot variations occur, so the measured samples should come from adjacent parts of the same boule if the actual flight article cannot be tested. In addition to the trapped-particle radiation, decay from materials which become radioactive under such bombardment must also be considered (primarily if it is part of the detector assembly). The sapphire prism light emission is acceptable (both particles and ultraviolet light produce fluorescence) because it is distant enough from the detectors that the direct illumination of the Digicons is small, and it is sufficiently defocused that light transmitted by the optical train is small also. The prism should never produce detectable levels of diffuse straylight background. The detectors are another matter. Fluorescence from the windows would be the major (and unacceptable) source of instrumental background if not suppressed. We use the 512-element diode array as self-anticoincidence detectors, relying on the circumstance that such fluorescence produces a simultaneous (by FOS timescales) burst of photoelectrons. Such bursts can be eliminated by enabling a software-selectable threshold which rejects any frame of data in which the sum of counts over a selected set (generally, all operational) of channels exceeds the software limit. With this burst noise rejection scheme operating, we expect fluorescence to contribute less than 0.001 count/diode/sec outside the South Atlantic Anomaly (SAA). Inside the SAA, such noise may be much greater, and it may not be possible to observe at all (the software may eliminate all data if noise bursts occur too frequently).

The dominant instrumental noise is expected to be the thermionic photocathode emission from each Digicon. During ST operation, the photocathode temperatures are calculated to lie between -10C and -28C. At the warm end of this range, the red Digicon noise has been measured to lie between 0.001 and 0.002 counts/diode/sec. At -10C, the blue detector background is about 0.0005 counts/diode/sec.

Electromagnetic disturbances, if severe enough, can cause the FOS electronics to produce spurious counts. All the ST instruments including the FOS incorporate normal good engineering practice -- single-point grounds to eliminate ground loops, shielding from conducted and radiated electrical fields, etc. -- and, of course, each instrument's production of electromagnetic interference is controlled. Additional protection for the FOS is provided by the burst-noise rejection scheme discussed above. Still, such sources of noise can only be eliminated with certainty at the ST integration level by thorough testing.

Thus, all instrumental background noise sources are expected to be less than our goal of 0.002 counts/diode/sec (outside the SAA).

4.2 Dynamic range. The minimum detectable source levels are set by instrumental background, while the maximum accurately measurable source levels are determined by the response times of the FOS electronics. Figure 4.2-1 compares the detected (apparent) rate to the true input rate for a typical channel of the FOS. The true rate can be derived

from the apparent rate up to at least a true rate of 5×10^4 counts/channel/sec (and, perhaps, to 10^5 counts/diode/sec). This enormous dynamic range, at least 2.5×10^7, means that sources over a range of 18 magnitudes in apparent luminosity can be observed with the FOS. (However, the accessible magnitude ranges are reduced by non-flatness of the spectrum, of course.)

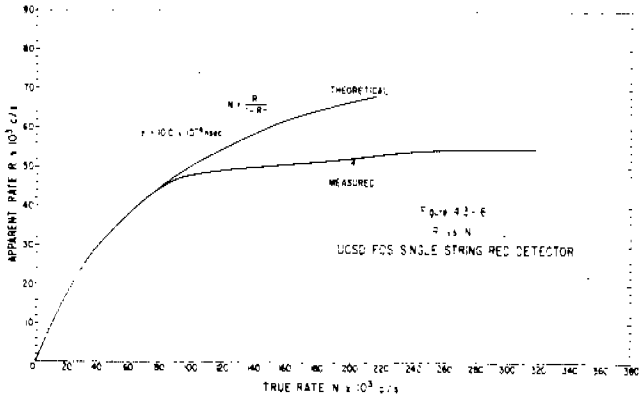

FIGURE 4.2-1. Measured versus true rates.

4.3 Instrument profile. The ability to resolve closely spaced spectral features is related to the instrument response-profile (to monochromatic input) at small separations (the peak), while the ability to detect weak spectral features is limited by the long distance response profile (the wings). The peak of the response profile is dominated by the nearly-50μ width of the Digicon diodes along the dispersion direction. The wings of the profile result primarily from scattered light due to the dispersers. A typical response profile, measured with a 50μ exit slit for one of the flight gratings, is presented in Figure 4.3-1. The results fully meet out desires, with far-field scattered light below 10^{-4} times the peak amplitude. One still remaining uncertainty is that we have not yet been able to measure the profiles of the most ultraviolet gratings, whose scattering properties may be worse.

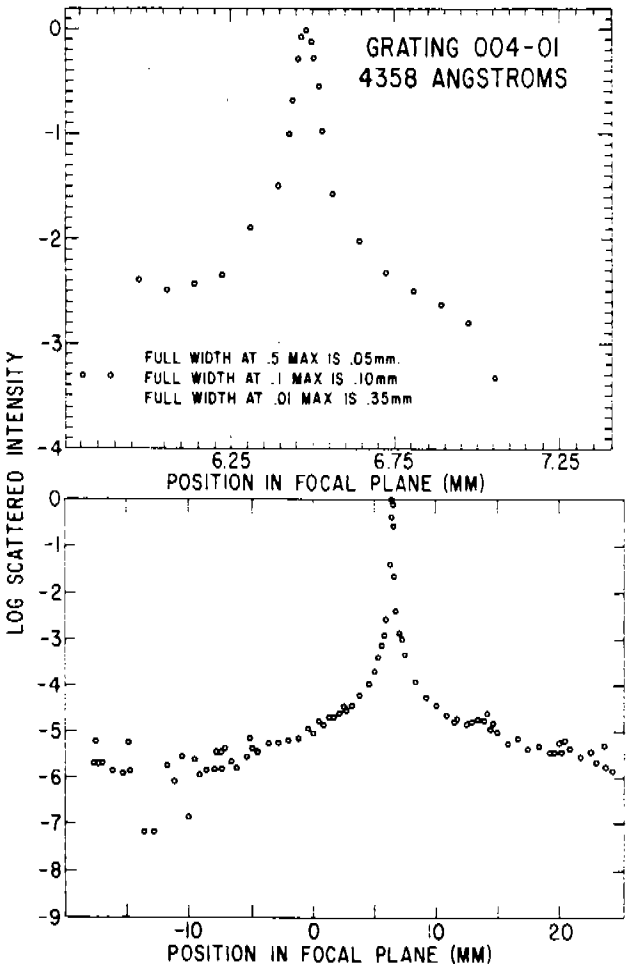

FIGURE 4.3-1. Upper figure displays peak scattered light profile of FOS flight grating; lower figure shows wings of profile. Measurement used 50 micron exit slit to match Digicon diode size.

4.4 Efficiencies. The total sensitivity of the spectrograph is strongly dependent upon the performance of the three least-efficient components in the optical train: 1) the dispersers, 2) the detectors, and 3) the polarizer.

Figures 4.4-1 and 4.4-2 display the fraction of incoming unpolarized light which is directed to the first-order focused spectrum by the moderate-and low-resolution dispersers. The high efficiency of the prism was expected. However, Hyperfine Inc. exceeded even our optimistic expectations in ruling the FOS flight gratings. With peak efficiencies over 50% in the ultraviolet and reaching 75% in the red, these concave gratings are the best produced of which we are aware. Figure 4.4-3 simply illustrates that the grating efficiency is not a strong function of the polarization of the incoming light.

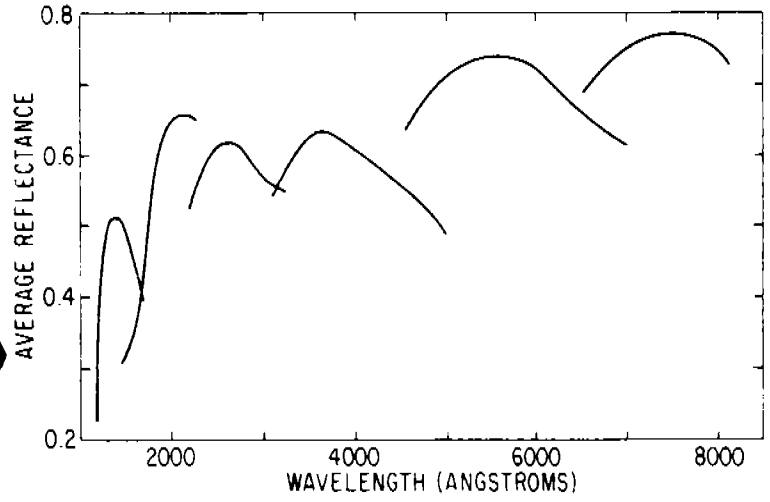

FIGURE 4.4-1. First-order efficiencies of FOS flight moderate-resolution gratings.

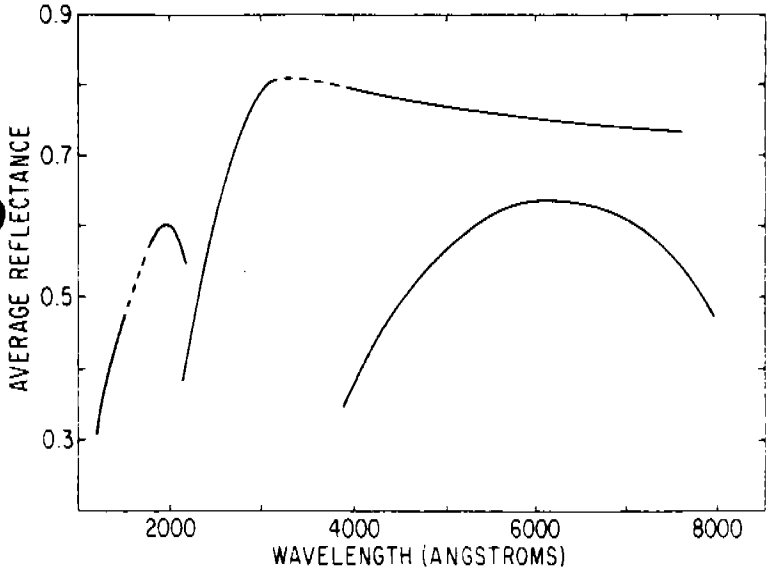

FIGURE 4.4-2. Efficiencies of FOS flight low-resolution dispersers: UV grating, prism, red grating.

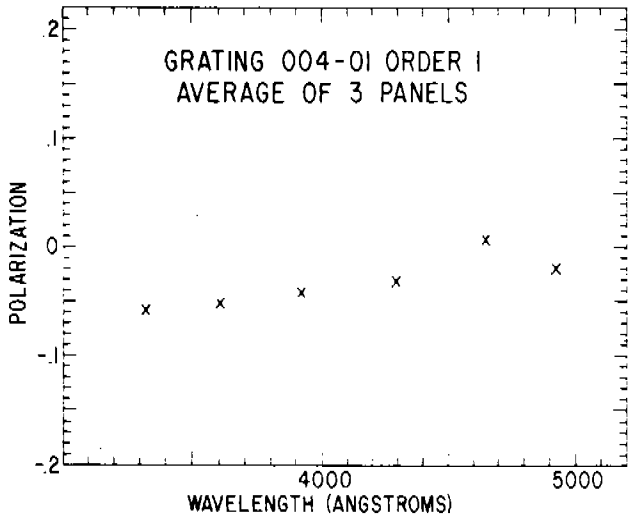

FIGURE 4.4-3. Polarization produced by flight FOS grating.

The response of the detectors has also been highly gratifying to us. The Digicons, produced by Electronic Vision Systems Division of Science Applications Incorporated, not only meet the stringent background noise requirements discussed in Section 4.1, but provide high quantum efficiency coverage from the magnesium-fluoride cutoff in the ultraviolet to the red photocathode dropoff in the near-infrared. Figure 4.4-4 shows the quantum efficiencies of the two flight detectors. Peak efficiency of the blue Digicon is just under 20%, of the red Digicon about 25%.

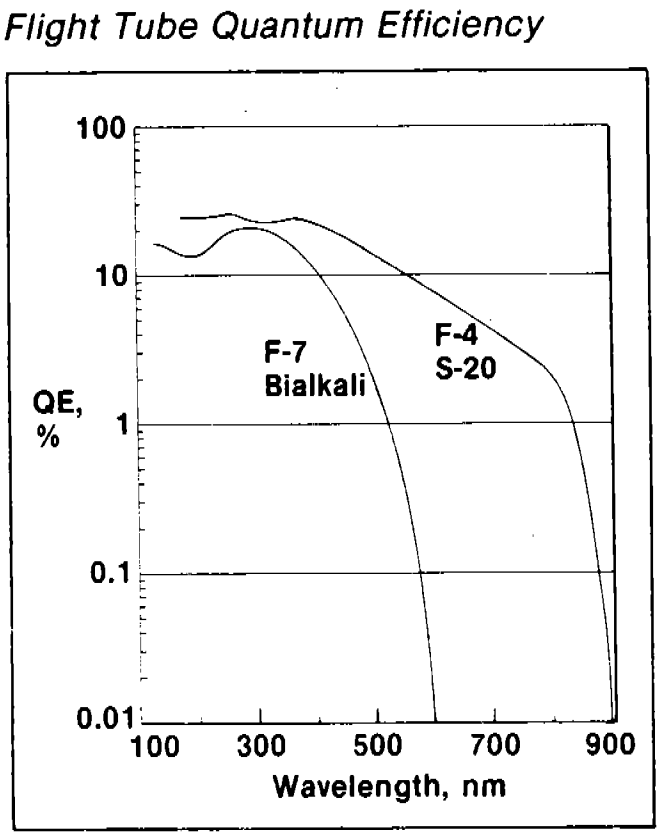

FIGURE 4.4-4. Quantum efficiencies of the two FOS flight detectors. Both produce under 0.002 counts/diode/sec noise at -10C.

The sensitivity of the polarizer depends both upon its throughput efficiency and its modulation efficiency (refer to Angel and Allen, 1982 for a detailed discussion of the FOS polarizer). The transmission efficiency of the complete polarizer rises from about 20% at Lyman α to around 60% at 160 nm, and thence rises more slowly to just over 80% at 240 nm. Because, at any given time, the detector can observe only one of the two spectra produced by the polarizer, another factor of two loss in practical throughput occurs. Finally, Table 4.4-1 lists the modulation efficiencies for each of the two waveplates. Note that the polarizer is sensitive to both linear and circular polarization over nearly the entire wavelength range of the FOS.

TABLE 4.4-1
Retardations of the Flight Waveplates

λ(Å)	Waveplate A δ	Waveplate A Efficiency linear	Waveplate A Efficiency circular	Waveplate B δ	Waveplate B Efficiency linear	Waveplate B Efficiency circular
1175	-108°	.65	.95	-93°	.53	1.00
1200	100°	.59	.98	0°	0	0
1216	215°	.91	.57	90°	.50	1.00
1250	360°	0	0	151°	.97	.33
1300	460°	.59	.98	228°	.83	.74
1350	482°	.76	.85	247°	.70	.92
1400	485°	.79	.82	250°	.67	.94
1450	480°	.75	.87	241°	.74	.87
1500	468°	.65	.95	238°	.76	.85
1600	439°	.85	.98	226°	.85	.72
2537	251°	.66	.94	123°	.77	.86
3650	163°	.98	.29	84°	.45	.99
6328	95°	.54	.99	43°	.13	.68

4.5 System performance. We can combine the measured performance parameters just discussed with the anticipated properties of the ST to calculate the expected on-orbit capability of the ST plus FOS. To indicate the system response, we consider observations using the quarter-arcsecond aperture. Figure 4.5-1 then illustrates the system sensitivity function versus wavelength for spectroscopic and spectropolarimetric observations. For moderate- and low-resolution spectroscopy, Figures 4.5-2 and 4.5-3 convert this into a conservative measure of limiting V magnitudes for a variety of astronomically relevant flux distributions. It is encouraging that acceptable quality (signal/noise = 5) spectra can be obtained in only one hour of integration down to about 22nd magnitude at resolution R = 1200, down to about 24th magnitude at R = 200, and (with the prism) down to nearly 26th magnitude (low and nonuniform resolution). Nor are these truly limiting; heroic observations can go 1.75 magnitudes fainter before instrumental noise dominates the signal. A significant exception to this is in the low-resolution mode. For the cases depicted in Figure 4.5-3, sky background is already significant using the prism at 400 to 500 nm. Of course, use of the 0.1 arcsecond aperture when possible will reduce sky levels another two magnitudes. (Sky brightness is not a problem in the moderate-dispersion mode.)

The polarizer goes less deep, of course. Table 4.5-1 tabulates the achievable accuracies in 10 nm bandpasses for a 15th magnitude AO star for ultraviolet polarimetry in a 20 minute exposure.

TABLE 4.5-1
Polarization Accuracy for AO Star, V=15, Exposure Time = 20 Minutes

(Å)	% Accuracy For Linear*	% Accuracy For Circular**
1216	6.4	5.8
1500	1.9	1.5
2000	0.89	0.74
2500	0.66	0.54
3000	0.63	0.58

* Standard deviation in Stokes parameter ratios Q/I and U/I
** Standard deviation in Stokes parameter V

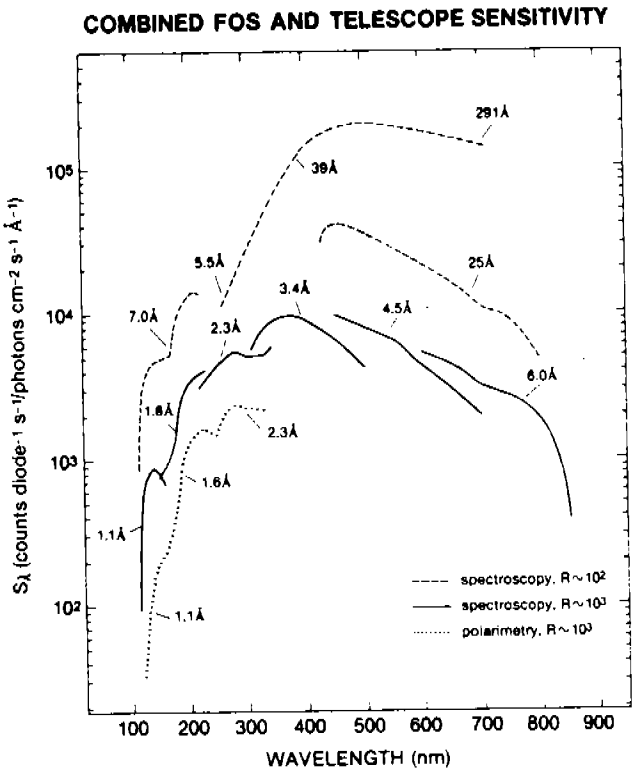

FIGURE 4.5-1. FOS + ST Sensitivity using the quarter arcsecond diameter entrance aperture.

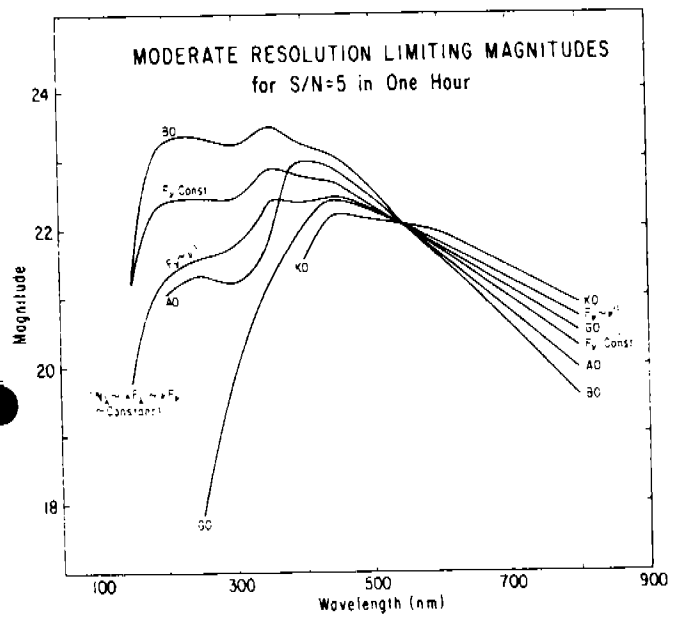

FIGURE 4.5-2. Limiting V Magnitudes for several flux distributions which produce 0.01 counts/sec/diode for moderate-resolution FOS spectroscopy (R=1200). With quarter-arcsecond aperture, night sky is negligible.

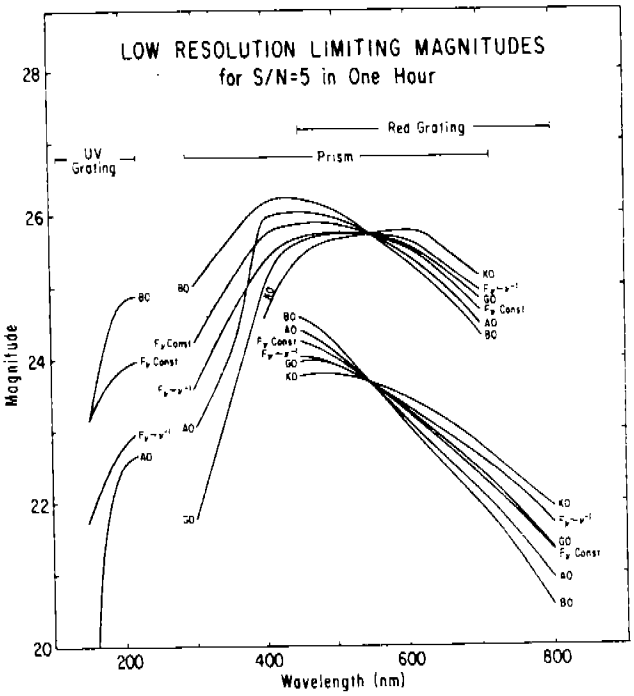

FIGURE 4.5-3. Limiting V magnitudes for low resolution FOS spectroscopy (R=200 for gratings, R strongly varying for prism). With quarter-arcsecond aperture, sky is significant only with the prism between 400 and 500 nm (e.g. for observing 25-26 magnitude objects).

5.0 References

Explicitly cited references are listed below:

1. Aanestad, P. A., Percell, E. N., 1973, Annual Rev. of Astro. and Astrophys., Vol. 11, p. 309.
2. Allen, R. G. and Angel, J. R. P., 1982, Proc. Society of Photo-Optical Instrumentation Engineers, Vol. 331, in press.
3. Angel, J. R. P., 1978, Ann. Rev. of Astro. and Astrophys., Vol. 16, p. 487.
4. Bahcall, J. N., 1980, in Scientific Research with the Space Telescope, IAU Coll. No. 54, NASA CP-2111, p. 215.
5. Gilra, D. P., 1972, The Scien. Results from the Orbit Astro. Obs., A. D. Code, Ed., p. 295 (NASA ST-310).
6. Harms, R. J. et al., 1979, Proc. Society of Photo-Optical Instrumentation Engineers, Vol. 183, p. 74.
7. Moore, C. E., 1950, An Ultraviolet Multiplet Table, Circ. of the NBS 488, Section 1.
8. Osterbrock, D. E., 1963, Planet. Space Sci., Vol. 11, p. 621.
9. Wagoner, R. V., 1980, in Physical Cosmology, Les Houches, Session XXXII, 1979, p. 179.
10. Weast, C. R. ed., 1968, CRC Handbook of Chemistry and Physics, 49th Edition, p. E-71.

Other general references describing features of the FOS include:

1. Bahcall, J. N. and O'Dell, C. R., 1980, in Scientific Research with the Space Telescope, IAU Coll. No. 54, NASA CP-2111, p. 5.
2. Ginaven, R. O. et al., 1981, Proc. Society of Photo-Optical Instrumentation Engineers, Vol. 290, p. 81.
3. Harms, R. J. et al., 1982, Proc. Society of Photo-Optical Instrumentation Engineers, Vol. 331, in press.
4. Leckrone, D. S., 1980, Publ. Astronomical Society of the Pacific, Vol. 92, p. 5.